Applied Ocean Research 93 (2019) 101965

Contents lists available at ScienceDirect

Applied Ocean Research

journal homepage: www.elsevier.com/locate/apor

Consistent expressions for the free-surface Green function in finite water depth

Ed Mackay

College of Engineering, Mathematics and Physical Sciences University of Exeter TR10 9FE, UK

ARTICLE INFO

Keywords:
Green function
Frequency domain
Zero frequency
Infinite frequency
Asymptotic analysis

ABSTRACT

Fast and accurate computation of the free-surface Green function is of key importance for the numerical solution of linear and second-order wave-structure interaction problems in three dimensions. Integral and series expressions for the Green function are derived for which the limiting values for zero and infinite frequency are consistent with the zero and infinite frequency Green function defined in terms of infinite series of Rankine image sources. The integral expressions presented here have the advantage that they are slowly varying with the non-dimensional wave frequency, making them more efficient to approximate compared with previous expressions.

1. Introduction

The boundary element method (BEM) is often used to solve linear and second-order wave-structure interaction problems in three dimensions [1]. BEM models use Greens theorem together with a suitable Green function to formulate an integral equation for the velocity potential over the surface of a body (or bodies). The integral equation is solved by discretising the body surface into a number of panels to formulate a linear system of equations which can be solved to yield the velocity potential, from which various hydrodynamic properties can be derived. The free-surface Green function $G(\mathbf{P}, \mathbf{Q})$ describes the linearised velocity potential at point $\mathbf{P} = (x, y, z)$ due to wave motions from a pulsating source at point $\mathbf{Q} = (\xi, \eta, \zeta)$. In a BEM model, the Green function and its gradient must be calculated between each pair of panels in the mesh. Meshes for complex geometries typically require $O(10^3) - O(10^4)$ panels, requiring $O(10^6) - O(10^8)$ evaluations of the Green function at each frequency. The use of the high-order method, where panels are represented using curved surfaces, can reduce the number of panels required to achieve mesh convergence [2]. However, in the high-order method, multiple evaluations of the Green function are required over each panel. Efficient evaluation of the Green function is therefore a key element in the computational efficiency of BEM models.

The calculation of the free-surface Green function in infinite water depth has received considerable attention in the literature, e.g. [3–30]. Efficient and accurate methods for calculating the infinite-depth Green function have been proposed by numerous authors. The approaches taken include polynomial approximation [17,18], eigenfunction expansion [20], representation in terms of ordinary differential equations [23,24,30] or approximation in terms of standard functions [25,26].

A series expansion of the finite-depth Green function was introduced by John [4]. Newman [14] noted that the convergence of the series is dependent on the ratio R/h, where $R = \sqrt{(x-\xi)^2 + (y-\eta)^2}$ is the horizontal separation between the source and field point and h is the water depth. For larger values of R/h the series provides an efficient means to calculate the Green function, with $6h/R$ terms required to achieve 6-decimal accuracy [14]. For smaller values of R/h the series is slow to converge and in the limiting case $R = 0$ the series is divergent. Pidcock [31] proposed various series expansions which are valid in the near field provided that the wavenumber is small (see [32]). The integral definition of the Green function given by John [4] is valid for all wavenumbers and values of R/h, but is slow to compute. Various methods have been proposed to compute the finite-depth Green function in the near field with greater efficiency (e.g. [14,16,18,32–38]). These methods all require the numerical evaluation of one or more integrals, which results in large computation times.

In principle, to reduce the computational time, the integrals defined in [14,16,18,32–38] could all be pre-calculated and approximated in some way, such as interpolation of lookup tables or polynomial approximation. However, the resolution required for the lookup table or the number of terms in the polynomial approximation will depend on the smoothness of function being interpolated. Newman [17] noted that the condition number of the linear systems solved in BEM models is often $O(100)$ and therefore recommended that the approximation of the Green function should achieve either a relative or absolute error of less

E-mail address: e.mackay@exeter.ac.uk.

https://doi.org/10.1016/j.apor.2019.101965
Received 24 May 2019; Received in revised form 12 September 2019

than 10^{-6}. To achieve this accuracy with low computational cost, the functions that are approximated should be as smoothly-varying as possible.

For time-domain calculations where the hydrodynamic forces are calculated using Cummins' equation [39] it is necessary to calculate the added mass at infinite frequency and an integral of the radiation damping over frequencies from zero to infinity. It is therefore important to have accurate expressions for the Green function for all frequencies from zero to infinity.

Newman [14] proposed a method for expressing the finite-depth Green function as the sum of Rankine sources, the infinite-depth Green function and a smoothly varying residual component which is amenable to polynomial approximation throughout most of the domain. The method described in [14] requires four evaluations of the infinite-depth Green function. Newman [17] mentioned an improved approach, requiring only a single evaluation of the infinite depth Green function, but did not provide details. A similar approach to that outlined in [17] was described in detail by Chen [18]. The integrals that are approximated in Newman and Chen's methods are functions of three non-dimensional variables (R/h, $|z \pm \zeta|/h$, Kh), where K is the infinite-depth wavenumber. The integrals approximated in Newman and Chen's methods have a large variability in magnitude at lower values of the non-dimensional wavenumber Kh and are singular in the limit $Kh \to 0$. Moreover, the limits of the integrals for $K \to 0$ and $K \to \infty$ are not consistent with the integral representation of the Green function at $K = 0$ and $K = \infty$.

In this work we follow a similar method to that described by Chen [18] to develop expressions which are consistent with the limiting form at $K = \infty$. The finite depth Green function has a singularity as $K \to 0$, so it is not possible to derive an expression which is completely consistent with the zero-frequency Green function. However, it is shown below that the singular component is independent of the spatial variables and is a function of Kh only. In this work we derive an expression where the singular component is separated, so that the spatial component has a limit that is consistent with the zero-frequency Green function. The new expressions also have the advantage that they are more slowly varying with the non-dimensional frequency Kh, making them more efficient to approximate. Following Newman [17] and Chen [18], triple Chebyshev polynomials are used to approximate the integrals that are derived in this work. This provides an efficient means for calculating the Green function in the domain $R/h \leq 1$ and has the advantage that the partial derivatives can be computed using the same approximation, with minimal additional computational cost.

In the domain $R/h > 1$, John's series expansion of the Green function is used. We propose a simple modification to the expression, which improves the numerical accuracy for high values of K and makes the limiting value consistent with the series expression for the Green function at infinite frequency. The code for calculating the Green function using the Chebyshev approximations and series definitions described here are available at https://github.com/edmackay/GreenFunction.

The paper is organised as follows. Section 2 presents the derivation of the new integral expressions. The modified form of John's series expansion for the finite-depth Green function is presented in Section 3. The limiting forms of the finite-depth Green function for $K = 0$ and $K = \infty$, defined in terms of infinite series of Rankine image sources, are presented in Section 4. An asymptotic analysis is presented in Section 5, which shows how the limiting forms of the expressions derived in Sections 2 and 3 are consistent with those presented in Section 4. The approximation of the new integral expressions in terms of Chebyshev polynomials is discussed in Section 6. Finally, conclusions are presented in Section 7.

2. Integral representation of the Green function

2.1. Definition of auxiliary functions

The free surface Green function $G(\mathbf{P}, \mathbf{Q})$ satisfies the Laplace equation in the fluid domain, the free-surface and seabed boundary conditions, given by

$$\nabla^2 G = \frac{1}{4\pi}\delta(x-\xi)\delta(y-\eta)\delta(z-\zeta), \tag{1}$$

$$\frac{\partial G}{\partial z} - KG = 0 \quad \text{on} \quad z = 0, \tag{2}$$

$$\frac{\partial G}{\partial z} = 0 \quad \text{on} \quad z = -h, \tag{3}$$

where $\delta(\cdot)$ is the Dirac delta function. A time dependence of $e^{i\omega t}$ is assumed throughout. Newman [14] and Chen [18] showed that the finite depth Green function can be written as the sum of Rankine sources, the deep water Green function and a function of three non-dimensional variables. It is useful to begin by defining the distance terms in the Rankine sources as

$$\begin{aligned} r_j &= \{R^2 + v_j^2\}^{1/2}, & R &= \{(x-\xi)^2 + (y-\eta)^2\}^{1/2}, \\ v_1 &= |z-\zeta|, & v_2 &= z+\zeta+2h, \\ v_3 &= |z+\zeta|, & v_4 &= z-\zeta+2h, \\ v_5 &= \zeta - z + 2h, & v_6 &= z+\zeta+4h. \end{aligned} \tag{4}$$

Non-dimensional variables are defined as

$$\begin{aligned} A &= \frac{R}{h}, & B_j &= \frac{v_j}{h}, \\ X &= KR, & V_j &= Kv_j, \\ H &= Kh. \end{aligned} \tag{5}$$

A sketch of the definition of the variables is shown in Fig. 1. r_1 is the distance from $\mathbf{Q}$ to $\mathbf{P}$. r_2 is the distance from $\mathbf{Q}$ to $\mathbf{P'}$, the image of $\mathbf{P}$ in the sea bed. r_3 is the distance from $\mathbf{Q}$ to $\mathbf{P''}$, the image of $\mathbf{P}$ in the free surface. The distances r_4, r_5 and r_6 can also be expressed in terms of images of $\mathbf{P'}$ and $\mathbf{P''}$ in the free surface and sea bed, but, for simplicity, these are not shown in Fig. 1. Note that $r_1 = 0$ when $\mathbf{P} = \mathbf{Q}$, $r_2 = 0$ when $\mathbf{P} = \mathbf{Q}$ and both points are on the sea bed and $r_3 = 0$ when $\mathbf{P} = \mathbf{Q}$ and both points are on the free surface. The distances r_4, r_5 and r_6 are always greater than zero, since v_4, $v_5 \in [h, 3h]$ and $v_6 \in [2h, 4h]$.

The derivation of the expressions proposed here is similar to the derivation given by Chen [18]. We start with the definition given by John [4] where the finite-depth Green function is expressed as

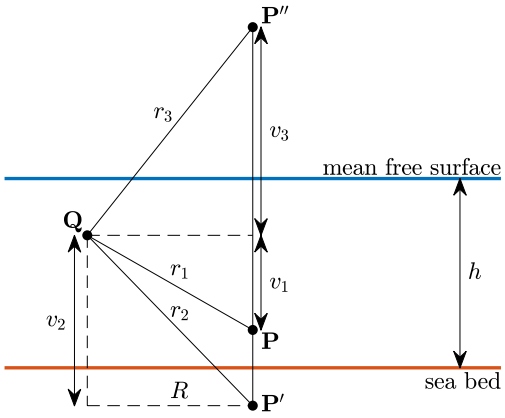

Fig. 1. Sketch of definition of variables.

$$G = \frac{1}{r_1} + \frac{1}{r_2} + \int_0^\infty \frac{2(k+K)\cosh(k(z+h))\cosh(k(\zeta+h))}{k\sinh(kh) - K\cosh(kh)} e^{-kh} J_0(kR)\mathrm{d}k, \tag{6}$$

where J_0 is the zero-order Bessel function of the first kind. The integrand of (6) has poles at solutions of the dispersion equation

$$k\tanh(kh) = K. \tag{7}$$

The dispersion equation has a single positive real solution, denoted k_0 and infinitely many purely imaginary solutions, denoted $\pm ik_n$, $n = 1, 2, \ldots$, where k_n are positive and ordered in increasing value. The integral in (6) is evaluated along a contour in the first quadrant complex plane to ensure outgoing waves in the far-field. The real part of G is given by

$$\mathrm{Re}(G) = \frac{1}{r_1} + \frac{1}{r_2} + \mathrm{PV}\int_0^\infty \frac{2(k+K)\cosh(k(z+h))\cosh(k(\zeta+h))}{k\sinh(kh) - K\cosh(kh)} e^{-kh} J_0(kR)\mathrm{d}k, \tag{8}$$

where PV denotes the Cauchy principal value. The imaginary part is given by the residue about the pole at k_0, which can be calculated for the entire domain $R/h \geq 0$ as the imaginary part of the series expansion, defined in Section 3. Substituting the non-dimensional variables into (8), expanding the hyperbolic functions in terms of exponentials and making the substitution $u = kh$, gives

$$\mathrm{Re}(G) = \frac{1}{r_1} + \frac{1}{r_2} + \frac{1}{h}\mathrm{PV}\int_0^\infty f(u,H)\left[e^{-u(2+B_1)} + e^{-u(2-B_1)} + e^{-u(2+B_2)} + e^{-u(2-B_2)}\right]J_0(uA)\mathrm{d}u, \tag{9}$$

where

$$f(u,H) = \frac{e^u}{2\cosh(u)}\cdot\frac{u+H}{u\tanh(u) - H} = \frac{u+H}{(u-H) - (u+H)e^{-2u}}. \tag{10}$$

The function $f(u, H)$ tends to 1 as $u \to \infty$, so the asymptotic value of the integrand can be subtracted by making use of the identity [40, Section 6.611]:

$$\int_0^\infty e^{-bx} J_0(ax)\mathrm{d}x = \frac{1}{\sqrt{a^2+b^2}}. \tag{11}$$

to obtain

$$\mathrm{Re}(G) = \sum_{j=1}^{6}\frac{1}{r_j} + \frac{1}{h}[G_1(A,B_1,H) + G_1(A,B_2,H)], \tag{12}$$

where

$$G_1(A,B,H) = \mathrm{PV}\int_0^\infty [f(u,H) - 1][e^{-u(2+B)} + e^{-u(2-B)}]J_0(uA)\mathrm{d}u. \tag{13}$$

Note that $B_1 \in [0, 1]$ and $B_2 \in [0, 2]$. The integral $G_1(A, B, H)$ converges for $B < 2$ but is divergent for $B = 2$. The value of G_1 shown in Fig. 2 for $A = 0$ and 1 and values of B between 0 and 1.8. G_1 is smoothly varying with H for $B \in [0, 1]$, but exhibits has large oscillations for $B > 1$. It will be shown in Section 5.2 that G_1 has a logarithmic singularity when both the source and field point coincide on the free surface (i.e. when $A = 0$ and $B_2 = 2$).

The behaviour of the integral can be improved by subtracting a closer asymptotic approximation for $f(u, H)$ as $u \to \infty$, given by

$$f(u,H) \to \frac{u+H}{u-H} \quad \text{as} \quad u \to \infty. \tag{14}$$

Define

$$\begin{aligned} G_2(A,B,H) &= \mathrm{PV}\int_0^\infty \left\{[f(u,H)-1]e^{-u(2+B)} + \left[f(u,H) - \frac{u+H}{u-H}\right]e^{-u(2-B)}\right\}J_0(uA)\mathrm{d}u, \\ &= \mathrm{PV}\int_0^\infty \{[f(u,H)-1]e^{-u(2+B)} + g(u,H)e^{-u(4-B)}\}J_0(uA)\,\mathrm{d}u \end{aligned} \tag{15}$$

where

$$g(u,H) = \frac{(u+H)^2}{(u-H)^2 - (u^2-H^2)e^{-2u}}. \tag{16}$$

Note that $g(u, H) \to 0$ as $u \to \infty$ so G_2 converges for $B \in [0, 2]$. Next, note that

$$\mathrm{PV}\int_0^\infty \left[\frac{u+H}{u-H} - 1\right]e^{-u(2-B_2)}J_0(uA)\mathrm{d}u = H\cdot F(X,V_3), \tag{17}$$

where

$$F(X,V) = 2\cdot\mathrm{PV}\int_0^\infty \frac{e^{-kV}}{k-1}J_0(kX)\mathrm{d}k. \tag{18}$$

The function $F(X, V)$ is the irregular component of the infinite-depth Green function [14]. The integral G_2 is shown in Fig. 3 for $A = 0$ and 1 and various values of B in [1,2]. It is evident that G_2 is smoothly-varying with all three variables A, B and H.

Finally, we can express the Green function as

$$\mathrm{Re}(G) = \sum_{j=1}^{6}\frac{1}{r_j} + \begin{cases} \frac{1}{h}[G_1(A,B_1,H) + G_1(A,B_2,H)] & 0 \leq B_2 \leq 1, \\ \frac{1}{h}[G_1(A,B_1,H) + G_2(A,B_2,H)] + K\cdot F(X,V_3) & 1 < B_2 \leq 2. \end{cases} \tag{19}$$

The expression for $B_2 > 1$ is also valid for $B_2 \in [0, 1]$. However, the advantage of using this form only in the domain $B_2 > 1$ is that the infinite depth component $F(X, V)$ does not need to be evaluated when $B_2 \leq 1$ and the integral G_2 only needs to be approximated for $B_2 \in [1, 2]$, which results in fewer terms being required in Chebyshev series. As mentioned in the introduction, the computation of the deep water component $F(X, V_3)$ has received considerable attention in the literature. The focus here is on the computation of the finite depth components G_1 and G_2.

Chen [18] derived similar expressions, but defined $H' = k_0 h$ rather than $H = Kh$ and did not make the substitution $u = kH$. The expressions given by Chen are:

$$\mathrm{Re}(G) = \sum_{j=1}^{6}\frac{1}{r_j} + \begin{cases} k_0[G_1'(A,B_1,H') + G_1'(A,B_2,H')] & 0 \leq B_2 \leq 1, \\ k_0[G_1'(A,B_1,H') + G_2'(A,B_2,H')] + K\cdot F(X,V_3) & 1 < B_2 \leq 2. \end{cases} \tag{20}$$

where

$$G_1'(A,B,H') = \mathrm{PV}\int_0^\infty [f'(k,H')-1]\left[e^{-kH'(2+B)} + e^{-kH'(2-B)}\right]J_0(kH'A)\mathrm{d}k, \tag{21}$$

$$G_2'(A,B,H') = \mathrm{PV}\int_0^\infty \left\{[f'(k,H')-1]e^{-kH'(2+B)} + g'(k,H')e^{-kH'(4-B)}\right\}J_0(kH'A)\mathrm{d}k, \tag{22}$$

and

$$f'(k,H') = \frac{k + \tanh H'}{(k - \tanh H') - (k + \tanh H')e^{-2kH'}}, \tag{23}$$

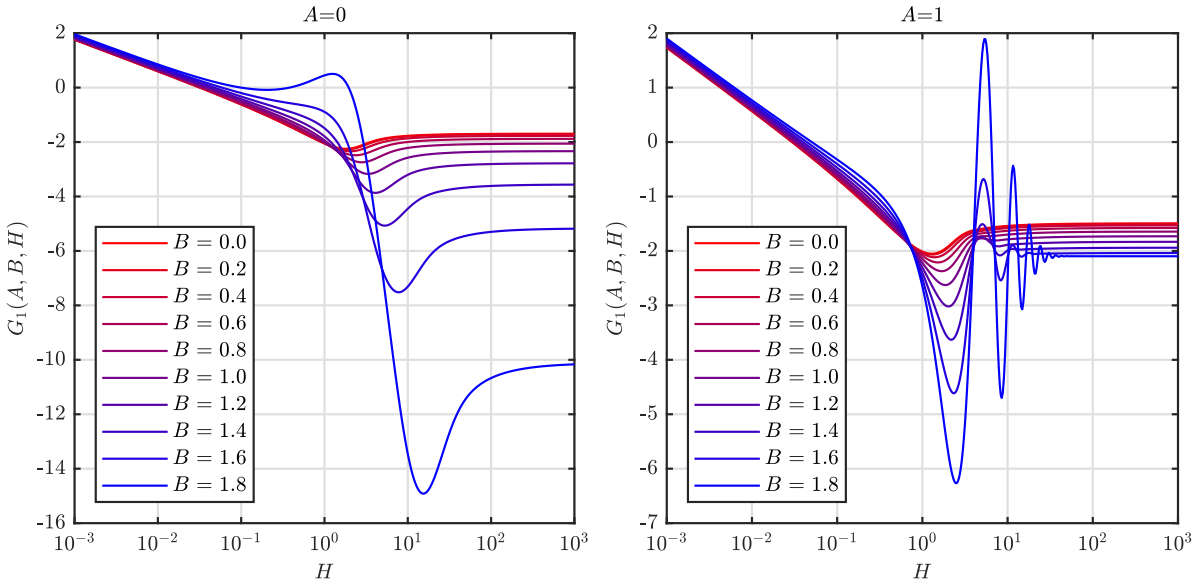

Fig. 2. The integral G_1 against H for $A = 0$ (left) and $A = 1$ (right) and various values of B.

$$g'(k, H') = \frac{(k + \tanh H')^2}{(k - \tanh H')^2 - (k^2 - \tanh^2 H')e^{-2kH'}}. \tag{24}$$

The integrals G_1' and G_2' are shown in Fig. 4 for $A = 0.5$ and various values of B. The pattern is similar for other values of A. It is evident that both G_1' and G_2' are singular as $H' \to 0$ and tend to zero as $H' \to \infty$. Note that by definition we have $H'G_1'(A, B, H') = G_1(A, B, H)$ and $H'G_2'(A, B, H') = G_2(A, B, H)$. So for given values of K and h, G_1' and G_2' are constant multiples of G_1 and G_2. However, expressing the Green function in terms of G_1 and G_2 has several advantages over expressing it in terms of G_1' and G_2'.

Firstly, in the expressions G_1 and G_2, the variables are separated so that the dependence on H is contained in the functions $f(u, H)$ and $g(u, H)$, which simplifies the asymptotic analysis. Furthermore, it will be shown in Section 2.2 that G_1 and G_2 can be decomposed into two functions, one which is finite for all values of H and the other that is a function of H only and contains the logarithmic singularity for $H \to 0$. In Section 5 it will be shown that the limiting forms of the Green function for $K = 0$ and $K = \infty$ can be derived from the limiting behaviour of G_1 and G_2. In contrast, as $K \to 0$ we have $G_1', G_2' \to \infty$ and as $K \to \infty$ we have $G_1', G_2' \to 0$, which makes the limiting behaviour harder to obtain.

The second advantage is that G_1 and G_2 are less variable with H and hence require fewer terms to approximate using Chebyshev polynomials. This is discussed further in Section 6.

2.2. Decomposition of auxiliary functions

From Fig. 2 it is evident that G_1 is singular for $H \to 0$. When $A = B = 0$, the product of the exponential and Bessel functions in (13) is equal to $2e^{-2u}$. We can subtract this component, so that the residual function is zero for all H when $A = B = 0$. Define

$$G_1(A, B, H) = L_1(A, B, H) + L_2(H), \tag{25}$$

where

$$L_1(A, B, H) = \text{PV} \int_0^\infty [f(u, H) - 1]\{[e^{-u(2+B)} + e^{-u(2-B)}]J_0(uA) - 2e^{-2u}\}\mathrm{d}u, \tag{26}$$

$$L_2(H) = \text{PV} \int_0^\infty [f(u, H) - 1]2e^{-2u}\mathrm{d}u, \tag{27}$$

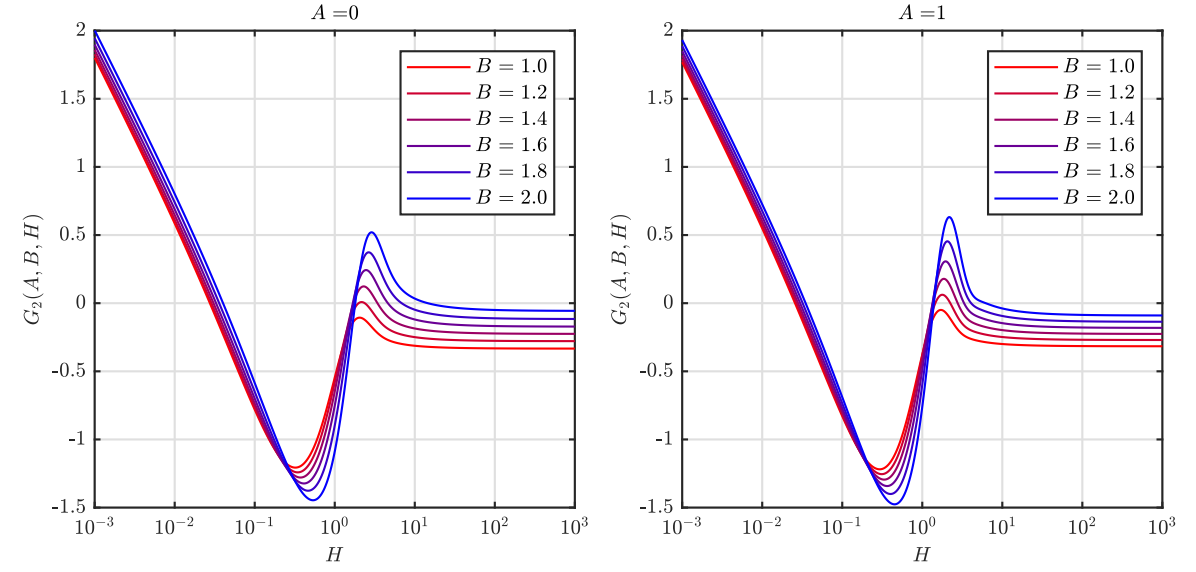

Fig. 3. The integral G_2 against H for $A = 0$ (left) and $A = 1$ (right) and various values of B.

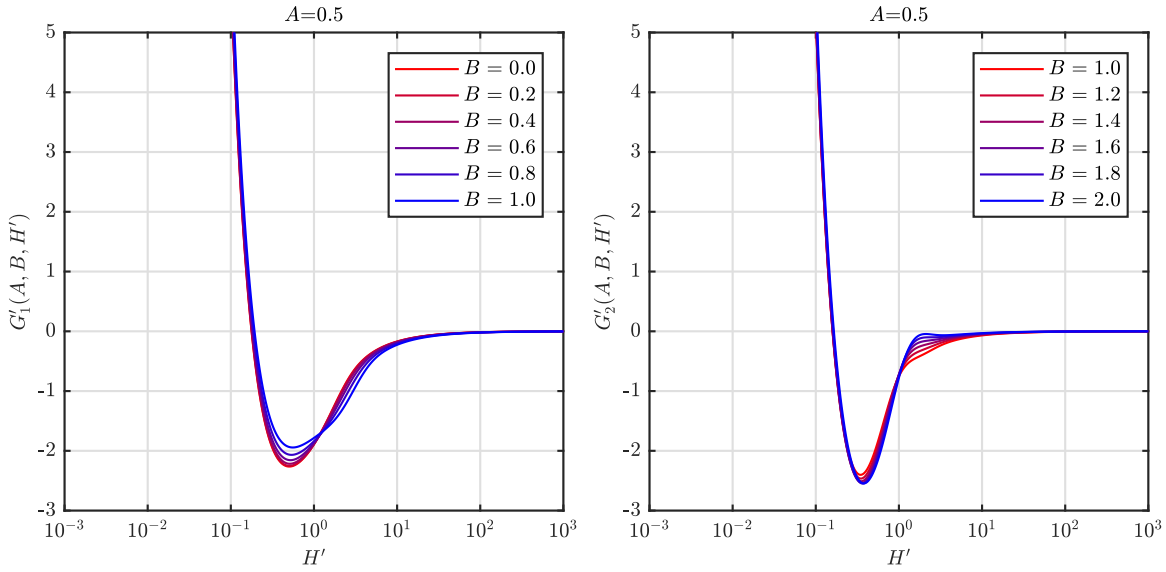

Fig. 4. The integrals G_1' (left) and G_2' (right) against H' for $A = 0.5$ and various values of B.

The integrals L_1 and L_2 are shown in Fig. 5 for $A = 0$, 0.5, 1 and various values of B. The integral L_2 is a function of H only, and contains the logarithmic singularity as $H \to 0$. The integral L_1 appears to tend to finite limits for $H \to 0$ and $H \to \infty$ and is smoothly varying with H. However, it is apparent that for $H > 1$ there is a greater variability in L_1 with A and B than for $H < 1$. Note that for $H \to \infty$ we have

$$f(u, H) \to -\frac{1}{1 + e^{-2u}}. \tag{28}$$

This suggests that for large H it would be more appropriate to define

$$G_1(A, B, H) = -\frac{2}{\sqrt{A^2 + (2 - B)^2}} - \frac{2}{\sqrt{A^2 + (2 + B)^2}} + L_3(A, B, H), \tag{29}$$

where

$$L_3(A, B, H) = \text{PV} \int_0^\infty [f(u, H) + 1][(e^{-u(2+B)} + e^{-u(2-B)}]J_0(uA)\text{d}u. \tag{30}$$

The integral L_3 is shown in Fig. 6 for $A = 0$ and 1 and various values of B. It is clear that this expression exhibits less variability with A and B than L_1 for the range of H shown. In this range it is not advantageous to subtract a component analogous to L_2, as L_3 is already finite in this range.

A similar decomposition can be used for the integral G_2 to subtract the singular component for $H \to 0$. In this case, G_2 is required for $B_2 \in [1, 2]$, so we define a residual function that is zero for $A = 0$ and $B = 1$ as

$$G_2(A, B, H) = M_1(A, B, H) + M_2(H), \tag{31}$$

where

$$M_1(A, B, H) = \text{PV} \int_0^\infty \{[f(u, H) - 1][e^{-u(2+B)}J_0(uA) - e^{-3u}] + g(u, H)[e^{-u(4-B)}J_0(uA) - e^{-3u}]\}\text{d}u, \tag{32}$$

$$M_2(H) = \text{PV} \int_0^\infty [f(u, H) - 1 + g(u, H)]e^{-3u}\text{d}u. \tag{33}$$

The integrals M_1 and M_2 are shown in Fig. 7. It is evident that M_1 tends to finite limits for $H \to 0$ and $H \to \infty$ and M_2 contains the logarithmic singularity. The variability in M_1 for higher values of H can be reduced in a similar way to that for L_1, by defining

$$G_2(A, B, H) = -\frac{2}{\sqrt{A^2 + (2 + B)^2}} + M_3(A, B, H), \tag{34}$$

where

$$M_3(A, B, H) = \text{PV} \int_0^\infty \{[f(u, H) + 1]e^{-u(2+B)} + g(u, H)e^{-u(4-B)}\}J_0(uA)\text{d}u. \tag{35}$$

The integral M_3 is shown in Fig. 8 for $A = 0$, $A = 1$ and various values of B. There is a small reduction in the variability with A and B compared to M_1.

For the Chebyshev approximations of the integrals, discussed in Section 6, we define

$$G_1 = \begin{cases} L_1(A, B, H) + L_2(H) & H \le 1, \\ L_3(A, B, H) & H > 1, \\ \quad - \dfrac{2}{\sqrt{A^2 + (2 + B)^2}} - \dfrac{2}{\sqrt{A^2 + (2 - B)^2}} & \end{cases} \tag{36}$$

$$G_2 = \begin{cases} M_1(A, B, H) + M_2(H) & H \le 1, \\ M_3(A, B, H) - \dfrac{2}{\sqrt{A^2 + (2 + B)^2}} & H > 1. \end{cases} \tag{37}$$

The integrals L_j and M_j ($j = 1, 2, 3$) are evaluated using contour integration to avoid numerical issues close to the poles in the integrand. The function $f(u, H)$ has a single positive real pole at $u_0 = k_0 h$ and infinitely many purely imaginary poles at $\pm u_n = \pm ik_n h$. For small values of H we have $u_0 \to \sqrt{H}$ and for large H we have $u_0 \to H$. In particular we have $u_0 \in [H, H + 0.3]$ for all H and $u_n \in [n\pi - 1/2, n\pi]$ for $n \ge 1$. The function $g(u, H)$ has the same poles as $f(u, H)$ and an additional pole at $u = H$. We are therefore free to define any contour of integration that avoids these poles. For the present work, the path of integration is defined (arbitrarily) as the line connecting the points $\{0, H + i, H + 1, \infty\}$, illustrated in Fig. 9. In this work, the integrals have been evaluated using vectorised adaptive quadrature [41] with an absolute tolerance of 10^{-10}.

3. Series representation of the Green function

John [4] showed that the finite-depth Green function can be expressed as a series given by

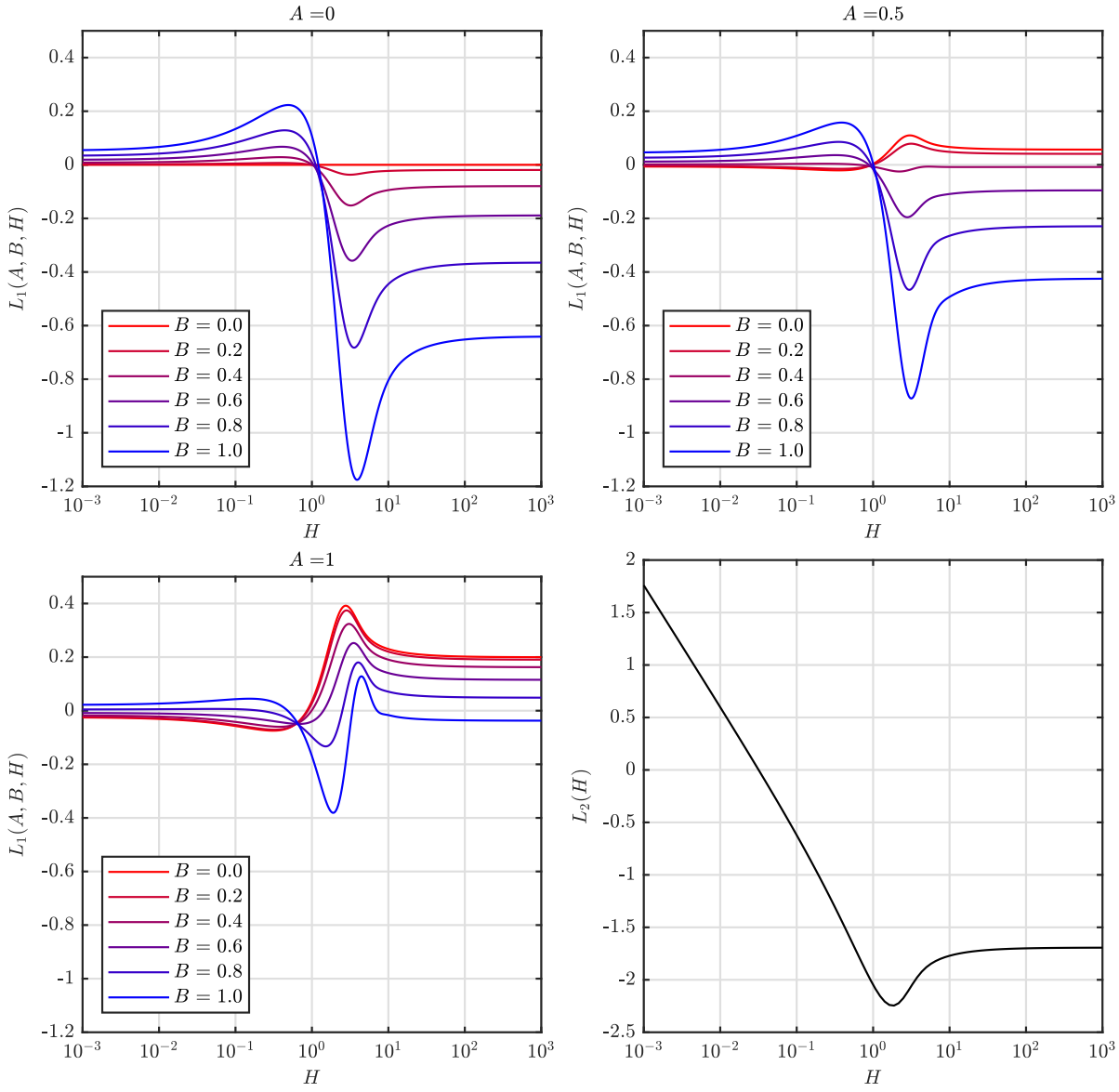

Fig. 5. The integrals $L_1(A, B, H)$ and $L_2(H)$ against H for various values of A and B.

$$G = -2\pi\frac{k_0^2-K^2}{(k_0^2-K^2)h+K}\cosh(k_0(z+h))\cosh(k_0(\zeta+h))(Y_0(k_0R)+iJ_0(k_0R)) + 4\sum_{n=1}^{\infty}\frac{k_n^2+K^2}{(k_n^2+K^2)h-K}\cos(k_n(z+h))\cos(k_n(\zeta+h))K_0(k_nR), \tag{38}$$

where Y_0 and K_0 are the zero-order Bessel functions of the second kind and modified second kind, respectively. Newman [14] noted that since $(n-\frac{1}{2})\pi \le k_n h \le n\pi$, for large n we have $K_0(k_nR) = O(\exp(-n\pi R/h))$. The rate of convergence of the series is therefore governed by the ratio R/h. For the domain $R/h > 1$, a maximum of $6h/R$ terms in the series are sufficient achieve 6-decimal precision.

When Kh is large, $k_0 \approx K$ and the fraction involving k_0 in (38) decreases exponentially, whilst the hyperbolic terms increase exponentially. To avoid numerical inaccuracies involved with multiplying very small and very large numbers, (38) can be rewritten using the relation

$$k_0^2 - K^2 = \frac{k_0^2}{\cosh^2(k_0h)}, \tag{39}$$

which can be derived from the dispersion Eq. (7). Substituting this into (38) and expanding the hyperbolic functions in terms of exponentials gives

$$G = -2\pi\frac{k_0^2}{(k_0^2-K^2)h+K}\cdot\frac{1}{(1+e^{-2k_0h})^2}\left[\sum_{j=3}^{6}e^{-k_0\nu_j}\right](Y_0(k_0R) + iJ_0(k_0R)) + 4\sum_{n=1}^{\infty}\frac{k_n^2+K^2}{(k_n^2+K^2)h-K}\cos(k_n(z+h))\cos(k_n(\zeta+h))K_0(k_nR). \tag{40}$$

In this form, the fraction involving k_0 increases linearly as $K \to \infty$ and the sum involving the exponential terms decreases exponentially (provided that $\nu_3 > 0$), which improves the accuracy of numerical computations.

4. Limiting forms in terms of series of rankine image sources

In the limiting cases of $K = 0$ and $K = \infty$ the free surface boundary condition (2) reduces to a homogeneous Neumann or Dirichlet

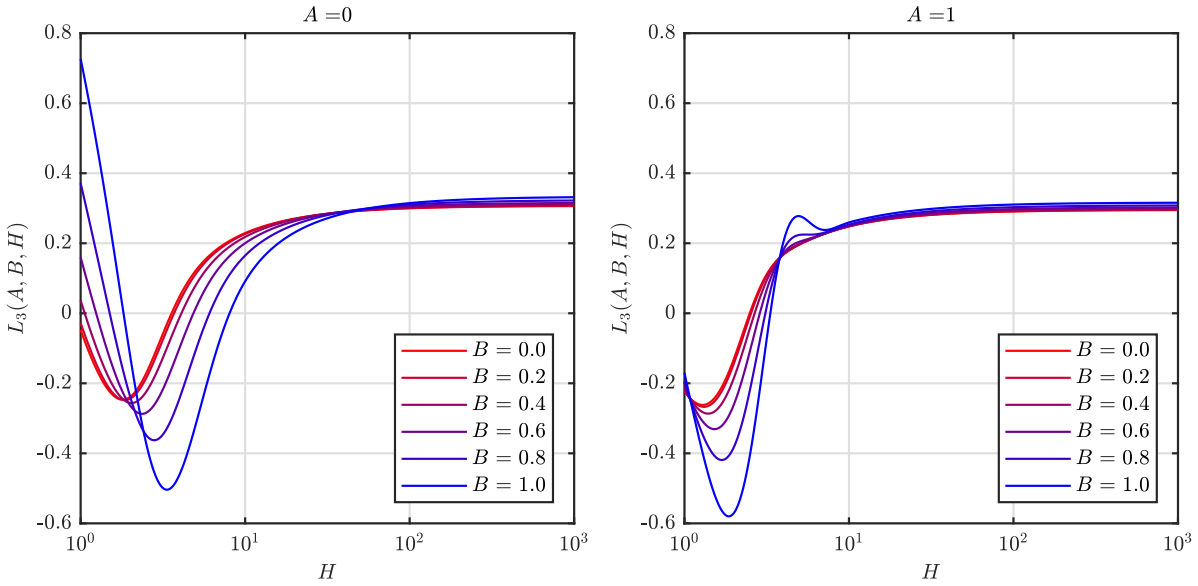

Fig. 6. The integral $L_3(A, B, H)$ against H for $A = 0$ (left) and $A = 1$ (right) and various values of B.

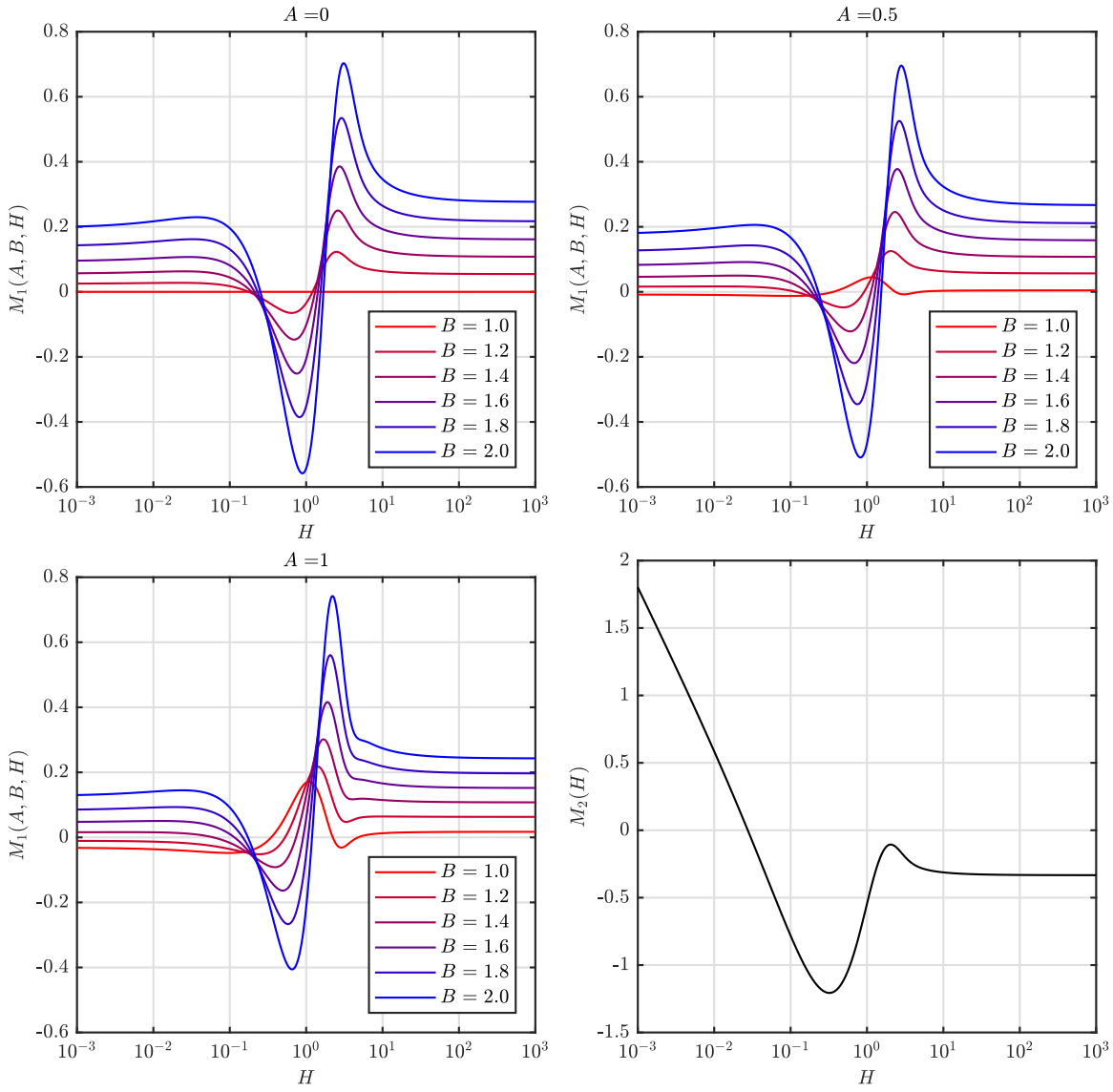

Fig. 7. The integrals $M_1(A, B, H)$ and $M_2(H)$ against H for various values of A and B.

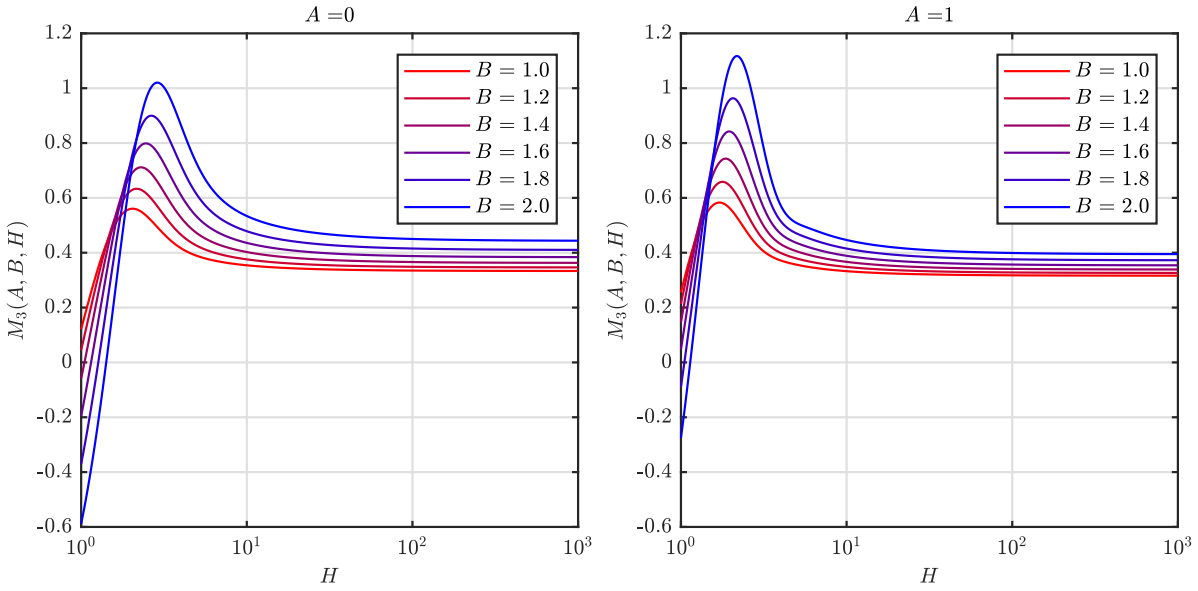

Fig. 8. The integral $M_3(A, B, H)$ against H for $A = 0$ (left) and $A = 1$ (right) and various values of B.

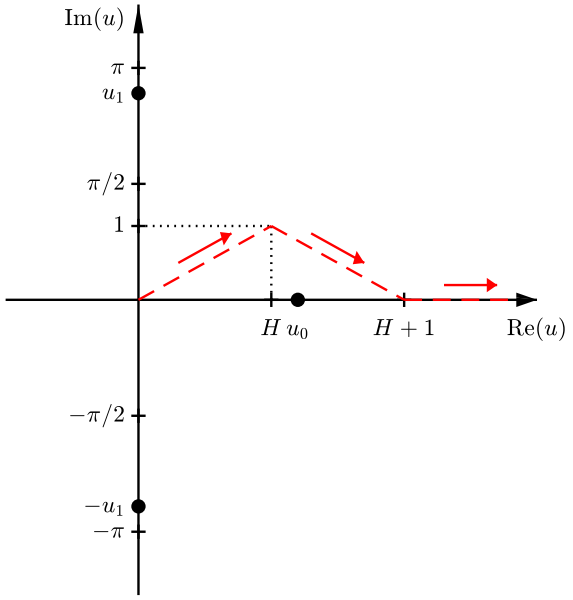

Fig. 9. Path of integration (red dashed line) for integrals L_j and M_j ($j = 1, 2, 3$). (For interpretation of the references to colour in this figure legend, the reader is referred to the web version of this article.)

condition:

$$\frac{\partial G}{\partial z}=0, \quad z = 0, K = 0, \tag{41}$$

$$G=0, \quad z = 0, K = \infty. \tag{42}$$

In these cases the finite-depth Green function can be expressed in terms of an infinite series of images of a Rankine source with respect to free surface and sea bed, defined as [17]

$$G_{\pm}(A, B) = \frac{1}{\sqrt{A^2 + B^2}} + \sum_{\substack{n=-\infty \\ n\neq 0}}^{\infty} (\pm)^n \left\{ \frac{1}{\sqrt{A^2 + (B + 2n)^2}} - \frac{1}{2|n|} \right\}. \tag{43}$$

The function $G_{\pm}$ is periodic in B, with G_+ having period 2 and G_- having period 4. There are therefore infinitely many combinations which satisfy the boundary conditions (41) and (42) together with the remaining conditions (1) and (3). Moreover, for the case $K = 0$, the Green function is only defined up to an arbitrary constant of integration. For consistency with the definition of the Green function presented in the previous sections, we define the finite-depth Green function at $K = 0$ and $K = \infty$ as

$$G_0 = \frac{1}{h}[G_+(A, B_1) + G_+(A, B_2) - 2\log(2)], \tag{44}$$

$$G_\infty = \frac{1}{h}[G_-(A, B_1) + G_-(A, B_2) - 2\log(2)], \tag{45}$$

where A and B_j are defined in (5).

The series in (43) are slow to converge. Newman [17] provided Fourier series and integral representations of $G_{\pm}$ as the basis for more efficient numerical calculations. The Fourier series are defined as

$$G_+=2\left[\sum_{n=1}^{\infty} \cos(n\pi B)K_0(n\pi A)\right] - \gamma - \log(A/4), \tag{46}$$

$$G_-=2\left[\sum_{n=0}^{\infty} \cos((n + \tfrac{1}{2})\pi B)K_0((n + \tfrac{1}{2})\pi A)\right] + \log(2), \tag{47}$$

where $\gamma \approx 0.577...$ is Euler's constant. Substituting these expressions into (44) and (45) gives

$$G_0 = -\frac{1}{h}\left(2\log\left(\frac{R}{2h}\right) + 2\gamma\right) + \frac{4}{h}\sum_{n=1}^{\infty} \cos\left(\frac{n\pi z}{h}\right)\cos\left(\frac{n\pi\zeta}{h}\right)K_0\left(\frac{n\pi R}{h}\right), \tag{48}$$

$$G_\infty = \frac{4}{h}\sum_{n=0}^{\infty} \sin\left(\left(n + \tfrac{1}{2}\right)\frac{\pi z}{h}\right)\sin\left(\left(n + \tfrac{1}{2}\right)\frac{\pi\zeta}{h}\right)K_0\left(\left(n + \tfrac{1}{2}\right)\frac{\pi R}{h}\right). \tag{49}$$

In the domain $R/h > 1$ the series converges to an error less than 10^{-6} with a maximum of 6 terms [17]. As with the case for $0 < K < \infty$, the series representation is slower to converge when R/h is small and it is more efficient to use an integral representation which can be approximated using Chebyshev polynomials. The integral representations are given by

$$G_{\pm}=(A^2 + B^2)^{-1/2} \pm (A^2 + (B + 2)^2)^{-1/2} \pm (A^2 + (B - 2)^2)^{-1/2} \pm L_{\pm}(A, B), \tag{50}$$

where

$$L_{\pm}(A, B) = \int_0^{\infty} \left\{ \begin{pmatrix} \text{cschu} \\ \text{sechu} \end{pmatrix} e^{-u}[\cosh(uB)J_0(uA) - 1] - 2e^{-2u}\cosh(uB)J_0(uA) \right\} \mathrm{d}u \quad . \tag{51}$$

Note that (50) has been corrected for a term ± 1 which appears erroneously in Eq. (6) of [17]. By expanding the hyperbolic functions in terms of exponentials and collecting terms, (51) can be rewritten as

$$L_{+} = \int_0^{\infty} \frac{1}{1 - e^{-2u}} \{[e^{-u(4-B)} + e^{-u(4+B)}]J_0(uA) - 2e^{-2u}\} \mathrm{d}u, \tag{52}$$

$$L_{-} = \log(2) + \int_0^{\infty} \frac{1}{1 + e^{-2u}} [e^{-u(4-B)} + e^{-u(4+B)}]J_0(uA) \mathrm{d}u. \tag{53}$$

If we define

$$L_0 = L_{+} - \log(2), \tag{54}$$

$$L_{\infty} = L_{-} - \log(2), \tag{55}$$

then substituting (50) into (44) and (45) gives

$$G_0 = \sum_{j=1}^{6} \frac{1}{r_j} + \frac{1}{h} \sum_{j=1}^{2} L_0(A, B_j), \tag{56}$$

$$G_{\infty} = \sum_{j=1}^{2} \frac{1}{r_j} - \sum_{j=3}^{6} \frac{1}{r_j} + \frac{1}{h} \sum_{j=1}^{2} L_{\infty}(A, B_j). \tag{57}$$

In infinite water depth (56) and (57) reduce to

$$\lim_{h\to\infty} G_0 = \frac{1}{r_1} + \frac{1}{r_3}, \tag{58}$$

$$\lim_{h\to\infty} G_{\infty} = \frac{1}{r_1} - \frac{1}{r_3}. \tag{59}$$

In the following section it will be shown that the limiting forms of the Green function defined here are consistent with the limiting forms of (19) and (40).

5. Asymptotic analysis

In this section we consider the behaviour of the expressions derived in Sections 2.2 and 3 for the cases

$$\begin{aligned} h &\to 0, \quad h \to \infty, \\ K &\to 0, \quad K \to \infty, \\ R, z, \zeta &\to 0, \quad R \to \infty. \end{aligned}$$

Firstly, in the case $h \to 0$, since G_1 and G_2 are finite for $K > 0$, from 19 we have $G \to \infty$. The remaining cases require more analysis and are considered in the following subsections.

5.1. Infinite depth

The limit of imaginary part of G can be derived from (40). We have

$$\lim_{h\to\infty} \frac{k_0^2}{(k_0^2 - K^2)h + K} = K, \tag{60}$$

$$\lim_{h\to\infty} \left[\frac{1}{(1 + e^{-2k_0 h})^2} \sum_{j=3}^{6} e^{-k_0 v_j} \right] = e^{-V_3}. \tag{61}$$

As noted before, the expression for $B_2 \in [1, 2]$ in 19 is valid for $B_2 \in [0, 2]$, so we have that

$$\lim_{h\to\infty} G = \frac{1}{r_1} + \frac{1}{r_3} + K\left[F(X, V_3) - 2\pi i e^{-V_3} J_0(X)\right], \tag{62}$$

which is the infinite depth Green function [14].

The infinite depth limit of the series (38) has been derived by Peter and Meylan [20]. The derivation for the series expression is more complex than for the integral expression and the reader is referred to [20] for details.

5.2. Source and field point coincide on free surface

The behaviour of the Green function on the free surface is important in the treatment of so-called 'irregular frequencies'. To remove the effects of irregular frequencies from radiation and diffraction problems, it is necessary to create a mesh over the internal free surface of the structure (see e.g. [42]). When the source and field point coincide on the free surface the Rankine components $1/r_1$ and $1/r_3$ are singular and can be subtracted from the Green function and integrated analytically over the panel using the method described in [43] (this method is applicable whenever $1/r_1$, $1/r_2$ or $1/r_3$ are singular). The integrals $G_1(A, B_1, H)$ and $G_2(A, B_2, H)$ are convergent and finite for $A \geq 0$, $B_1 \in [0, 1]$, $B_2 \in [0, 2]$ and $H > 0$. However, there is a singularity in $F(X, V_3)$ on the free surface when $X = V_3 = 0$. Newman [14] showed that for $X, V \to 0$ we have

$$F(X, V) \to 2(\log(2) - \gamma - \log(V + (X^2 + V^2)^{1/2})). \tag{63}$$

This logarithmic singularity can be subtracted and integrated analytically over the panel using the methods described in [44] or [45].

5.3. Zero frequency

5.3.1. Integral expressions

To derive expressions for the limiting values of G_1 and G_2 for $K \to 0$, we use the decomposition in terms of L_1, L_2, M_1 and M_2. The zero frequency limits of $f(u, H)$ and $g(u, H)$ are given by:

$$\lim_{H\to 0} f(u, H) = \frac{1}{1 - e^{-2u}}, \tag{64}$$

$$\lim_{H\to 0} g(u, H) = \frac{1}{1 - e^{-2u}}. \tag{65}$$

Substituting these expression into (26) and (32) gives

$$\begin{aligned} \lim_{H\to 0} L_1(A, B, H) &= \mathrm{PV} \int_0^{\infty} \frac{1}{1 - e^{-2u}} \{(e^{-u(4+B)} + e^{-u(4-B)})J_0(uA) \\ &\quad - 2e^{-4u}\} \mathrm{d}u \\ &= L_0 + 1 + \log(2), \end{aligned} \tag{66}$$

$$\begin{aligned} \lim_{H\to 0} M_1(A, B, H) &= \mathrm{PV} \int_0^{\infty} \frac{1}{1 - e^{-2u}} \{(e^{-u(4+B)} + e^{-u(4-B)})J_0(uA) \\ &\quad - e^{-5u} - e^{-3u}\} \mathrm{d}u \\ &= L_0 + 7/3 - \log(2). \end{aligned} \tag{67}$$

The second lines of (66) and (67) are obtained by substituting

$$\frac{2e^{-4u}}{1 - e^{-2u}} = \frac{2e^{-2u}}{1 - e^{-2u}} - 2e^{-2u}, \tag{68}$$

$$\frac{e^{-5u} + e^{-3u}}{1 - e^{-2u}} = \frac{2e^{-4u}}{1 - e^{-2u}} - e^{-3u} + 2e^{-2u} - 2e^{-u} + 2 - \frac{2}{1 + e^{-u}}. \tag{69}$$

Next we consider asymptotic behaviour of L_2 and M_2 for $H \to 0$. Write

$$f(u, H) = \frac{e^u}{2} p(u, H) \tag{70}$$

where

$$p(u, H) = \frac{u + H}{u\sinh(u) - H\cosh(u)}. \tag{71}$$

We can then write

$$L_2(H) = -1 + \mathrm{PV} \int_0^{\infty} p(u, H) e^{-u} \mathrm{d}u. \tag{72}$$

The function $p(u, H)$ has the following limiting form as $H \to 0$ (see Appendix A)

$$p(u, H) \to \frac{1}{2}\left(\frac{1+\sqrt{H}}{u-\sqrt{H}} + \frac{1-\sqrt{H}}{u+\sqrt{H}}\right) + (u+H)\left(\frac{1}{u\sinh(u)} - \frac{1}{u^2}\right). \tag{73}$$

Substituting this back into (72), the integral can be evaluated to give the limiting form for L_2 as $H \to 0$ as

$$L_2 \to \frac{1}{2}((1-\sqrt{H})e^{\sqrt{H}}\mathrm{E}_1(\sqrt{H}) - (1+\sqrt{H})e^{-\sqrt{H}}\mathrm{Ei}(\sqrt{H})) + \alpha H + \gamma - \log(2) - 1,$$

where numerical integration gives $\alpha \approx -0.1447$ and Ei and E_1 are exponential integrals, defined as ([46], Section 5.1.1)

$$\mathrm{Ei}(x) = -\mathrm{PV}\int_{-x}^{\infty}\frac{e^{-t}}{t}\mathrm{d}t, \quad \mathrm{E}_1(x) = \int_x^{\infty}\frac{e^{-t}}{t}\mathrm{d}t. \tag{74}$$

Using the approximations $\mathrm{Ei}(x) \approx -\mathrm{E}_1(x) \approx \log(x) + \gamma$ for small x ([46], Section 5.1.11), we obtain

$$L_2 \to -\log(H)/2 - \log(2) - 1 \quad \text{as} \quad H \to 0. \tag{75}$$

To obtain a similar expression for M_2, recall that

$$\frac{1}{h}[L_1(A, B_2, H) + L_2(H)] = \frac{1}{h}[M_1(A, B_2, H) + M_2(H)] + K{\cdot}F(X, V_3) \tag{76}$$

For $K \to 0$ we have $X, V \to 0$. From (63) we see that

$$\lim_{K\to 0} K{\cdot}F(X, V) = 0. \tag{77}$$

Therefore the asymptotic behaviour of $L_1 + L_2$ as $H \to 0$ is the same as that for $M_1 + M_2$. Hence

$$M_2(H) \to -\log(H)/2 + \log(2) - 7/3 \quad \text{as} \quad H \to 0. \tag{78}$$

Combining the limits (66), (67), (75) and (78), we obtain that

$$\lim_{K\to 0}\left[\mathrm{Re}(G) + \frac{1}{h}\log(Kh)\right] = G_0. \tag{79}$$

Hence the zero frequency limit of the real part of the Green function with the logarithmic singularity subtracted is equal to the zero frequency Green function defined in terms of series of Rankine image sources. In the following subsection it will be shown that the zero frequency limit of the imaginary part of the Green function is $-\pi/h$ and is independent of the values of R, z and ζ. As mentioned in the preceding section, for the case $K = 0$, the Green function is only defined up to an arbitrary constant. The constant imaginary part can therefore also be subtracted to yield a valid expression for zero frequency Green function as:

$$\lim_{K\to 0}\left[G + \frac{1}{h}\log(Kh) + \frac{i\pi}{h}\right] = G_0. \tag{80}$$

5.3.2. Series expressions

The asymptotic form of the series (38) for $K \to 0$ was given in [4], but is repeated here for completeness. First note that

$$k_0 \to \sqrt{K/h} \quad \text{as} \quad K \to 0, \tag{81}$$

$$k_n \to n\pi/h \quad \text{as} \quad K \to 0. \tag{82}$$

The limits of the coefficients in the series (40) are

$$\lim_{K\to 0}\frac{k_0^2}{(k_0^2 - K^2)h + K} = \frac{1}{2h}, \tag{83}$$

$$\lim_{K\to 0}\frac{k_n^2 + K^2}{(k_n^2 + K^2)h - K} = \frac{1}{h}. \tag{84}$$

The limits of the exponential terms in (40) are

$$\lim_{K\to 0}\left[\frac{1}{(1+e^{-2k_0h})^2}\sum_{j=3}^{6} e^{-k_0v_j}\right] = 1. \tag{85}$$

Using the asymptotic approximation for $x \to 0$ ([46], Section 9.1.8)

$$Y_0(x) \to \frac{2}{\pi}\left(\log\left(\frac{x}{2}\right) + \gamma\right), \tag{86}$$

and substituting the expressions above into (40) we obtain

$$\lim_{K\to 0}\left[G + \frac{1}{h}\log(Kh) + \frac{i\pi}{h}\right] = G_0. \tag{87}$$

Thus, the low frequency limit of the series definition of the Green function (40) with the logarithmic singularity and constant imaginary part subtracted, is equal to the series definition of the Green function for zero frequency derived in terms of series of Rankine image sources (48).

5.4. Infinite frequency

5.4.1. Integral expressions

As before, we consider limits of the functions $f(u, H)$ and $g(u, H)$. These are given by:

$$\lim_{H\to\infty} f(u, H) = \frac{-1}{1+e^{-2u}}, \tag{88}$$

$$\lim_{H\to\infty} g(u, H) = \frac{1}{1+e^{-2u}}. \tag{89}$$

Substituting these expression into (30) and (35) gives

$$\lim_{H\to\infty} L_3(A, B, H) = \lim_{H\to\infty} M_3(A, B, H) = L_\infty. \tag{90}$$

For the case where $B_2 > 1$ we also need to consider the infinite frequency limit of $F(X, V)$. From Eq. (8) in [14] we have

$$\lim_{K\to\infty} K{\cdot}F(X, V_3) = -\frac{2}{r_3}. \tag{91}$$

In the following subsection it will be shown that the infinite frequency limit of the imaginary part of the Green function is zero. Thus, for both cases $B_2 \le 1$ and $B_2 > 1$, we see that

$$\lim_{K\to\infty} G = G_\infty, \tag{92}$$

where G_∞ is defined in (57).

5.4.2. Series expressions

As before, we begin by considering the asymptotic behaviour of the wavenumbers:

$$k_0 \to K \quad \text{as} \quad K \to \infty, \tag{93}$$

$$k_n \to (n - \tfrac{1}{2})\pi/h \quad \text{as} \quad K \to \infty. \tag{94}$$

The limits of the coefficients in the series (40) are

$$\lim_{K\to\infty}\frac{k_0^2}{(k_0^2 - K^2)h + K} = K, \tag{95}$$

$$\lim_{K\to\infty}\frac{k_n^2 + K^2}{(k_n^2 + K^2)h - K} = \frac{1}{h}. \tag{96}$$

The limits of the exponential terms in (40) are

$$\lim_{K\to\infty}\left[\frac{1}{(1+e^{-2k_0h})^2}\sum_{j=3}^{6} e^{-k_0v_j}\right] = \begin{cases} 0 & \text{if} \quad v_3 > 0, \\ 1 & \text{if} \quad v_3 = 0. \end{cases} \tag{97}$$

Note that the fraction involving k_0 increases linearly as $K \to \infty$ whereas the sum involving the vertical terms decreases exponentially, provided that $v_3 > 0$, so the product of these terms tends to zero. For the case $v_3 > 0$, substituting the expressions above into (40) gives

$$\lim_{K\to\infty} G = G_\infty. \tag{98}$$

For this case, we see that the infinite frequency limit of (40) is equal to the series definition of the Green function derived in terms of Rankine image sources (49). In the case $\nu_3 = 0$ the limit of (40) does not exist. However, from (49) it can be seen that G_∞ and its partial derivatives are zero when $\nu_3 = 0$.

5.5. Far-field formulations

The far-field form of the finite depth Green function is used in the calculation of drift forces using the far-field method and other calculations involving the Kochin function. The far-field Green function is well known (see e.g. [47]), but is included here for completeness. By considering the asymptotic forms of the Bessel functions in (40), it can be shown that

$$\lim_{R\to\infty} G = \sqrt{\frac{8\pi k_0}{R}}\frac{k_0}{(k_0^2 - K^2)h + K}\cdot\frac{1}{(1+e^{-2k_0 h})^2}\left[\sum_{j=3}^{6} e^{-k_0\nu_j}\right]e^{-i(k_0 R+\pi/4)}. \tag{99}$$

For the infinite depth case, from (60) and (61) we have

$$\lim_{R,h\to\infty} G = \sqrt{\frac{8\pi K}{R}}e^{-\nu_3}e^{-i(KR+\pi/4)}. \tag{100}$$

6. Chebyshev approximation of integrals

The approximation of the infinite-depth component, $F(X, V)$, using Chebyshev polynomials is described in [17] and [18]. The focus here is on the approximation of the integrals L_j and M_j, $j = 1, 2, 3$. The theory is reviewed briefly here and further details can be found in e.g. [48].

The Chebyshev polynomials are defined by the recurrence relation

$$T_0(x) = 1, \tag{101}$$

$$T_1(x) = x, \tag{102}$$

$$T_{n+1}(x) = 2xT_n(x) - T_{n-1}(x). \tag{103}$$

Alternatively, the nth Chebyshev polynomial can be defined for $|x| \le 1$ as

$$T_n(x) = \cos(n\arccos(x)). \tag{104}$$

A real-valued function $f(x, y, z)$ which is regular in the domain $x, y, z, \in[-1, 1]$ can be expressed as a series of Chebyshev polynomials

$$f(x, y, z) = \sum_{p=0}^{\infty}\sum_{q=0}^{\infty}\sum_{r=0}^{\infty} a_{pqr}T_p(x)T_q(y)T_r(z). \tag{105}$$

Since $|T_j(x)| \le 1$ for $x \in [-1, 1]$, the function can be approximated to a specified error by truncating the series at a given minimum value of $|a_{pqr}|$. The coefficients a_{pqr} can be calculated from the orthogonality of the polynomials as:

$$a_{pqr} = \epsilon(p, q, r)\int_0^\pi\int_0^\pi\int_0^\pi f(\cos(\theta_1), \cos(\theta_2), \cos(\theta_3))\cos(p\theta_1)\cos(q\theta_2)\cos(r\theta_3)\mathrm{d}\theta_1\mathrm{d}\theta_2\mathrm{d}\theta_3, \tag{106}$$

where

$$\epsilon(p, q, r) = \frac{2^{(3-\delta_{0p}-\delta_{0q}-\delta_{0r})}}{\pi^3} \tag{107}$$

and δ_{ij} is the Kronecker delta function. The definitions in (105)–(107) reduce to expressions for functions of a single variable, by replacing the triple summations and integrals to single summations and integrals and defining $\epsilon(p) = 2^{(1-\delta_{0p})}/\pi$.

To represent the functions L_j and M_j, $j = 1, 2, 3$ in terms of Chebyshev polynomials, the domain is split into separate intervals of the variable H. In each region the variables A, B, H are mapped onto variables x, y, z and we define $f(x, y, z) = L_j(A, B, H)$ or $M_j(A, B, H)$. The mappings for A and B are defined as

$$x = 2A - 1, \tag{108}$$

$$y_1 = 2B_1 - 1 \tag{109}$$

$$y_2 = \begin{cases} 2B_2 - 1, & 0 \le B_2 < 1, \\ 2B_2 - 3, & 1 \le B_2 \le 2. \end{cases} \tag{110}$$

The mapping from H to z is dependent on the value of H and is described below.

Frequency-domain hydrodynamic calculations for a given geometry are typically carried out for a fixed water depth and the radiation and diffraction problems are solved for a single value of K (and hence a single value of H) at a time. The summation over r can therefore be made prior to the execution of the function, so that the calculations for a single frequency can be evaluated using a double summation:

$$f(x, y, z) = \sum_{p=0}^{N_p}\sum_{q=0}^{N_q} b_{pq}T_p(x)T_q(y), \tag{111}$$

where

$$b_{pq} = \sum_{r=0}^{N_r} a_{pqr}T_r(z). \tag{112}$$

The coefficients of the Chebyshev polynomials grow exponentially with the order of the polynomial, whilst the terms a_{pqr} typically decrease exponentially with the order of the polynomial. For high order representations it is numerically more accurate to use the trigonometric definition of $T_r(z)$ to evaluate (112) rather than the polynomial form defined using the recurrence relations.

Conversely, for the evaluation of the partial derivatives f_x and f_y, it is more convenient to rewrite (111) in terms of monomials

$$f(x, y, z) = \sum_{p=0}^{N_p}\sum_{q=0}^{N_q} c_{pq}x^p y^q, \tag{113}$$

where the coefficients c_{pq} are calculated from b_{pq} and the coefficients of the Chebyshev polynomials. The maximum values of N_p and N_q required for the integrals considered here are 11 and 10, respectively, so the polynomial form does not suffer from issues with numerical accuracy. The efficiency of the calculation is further improved by noting that A and B are independent of K and hence the terms x^p ($p = 1, \ldots, N_p$), y^q ($q = 1, \ldots, N_q$) need only be calculated once at the start of the program.

For each integral, the coefficients a_{pqr} have been calculated for a range of p, q and r such that for greater p, q or r we have $|a_{pqr}| < 10^{-7}$. The functions $L_2 + \log(H)/2$ and $M_2 + \log(H)/2$ are approximated for the full range $H \in [0, 1]$, with the values at $H = 0$ defined using (75) and (78) and defining $z = 2H - 1$. This requires 119 and 274 terms for L_2 and M_2, respectively. The number of terms required could be reduced by splitting the range of H into sub intervals. However, the series only needs to be summed for a single value of H at each frequency, compared to $O(10^6) - O(10^8)$ values of A and B for the other integrals, so splitting the domain would have negligible impact on computational speed.

For the integrals L_1 and M_1 the range of H is split into three domains. For $H \in [0, 0.1]$ we define $z = 20H - 1$ and define the values at $H = 0$ using the asymptotic expressions (66) and (67). For higher values of H we map $\log_{10}(H)$ linearly onto $[-1, 1]$ as this results in a smoother variation in the values of the function (see Figs. 5 and 7). The domain is split at $\log_{10}(H) = -0.5$. The upper limits of the summations in each domain are $(N_p, N_q, N_r) = (7, 7, 52)$, (8,8,7) and (9,9,9) for L_1 and $(N_p, N_q, N_r) = (6, 7, 72)$, (7,7,8) and (8,8,10) for M_1. As with the case for L_2 and M_2, the value of N_r is less important, since the summation (112) is calculated for a single value of z. After summation over r, the number of terms with $|b_{pq}| > 10^{-7}$ in each subdomain are 39, 49 and 58 for L_1 and 34, 35 and 43 for M_1.

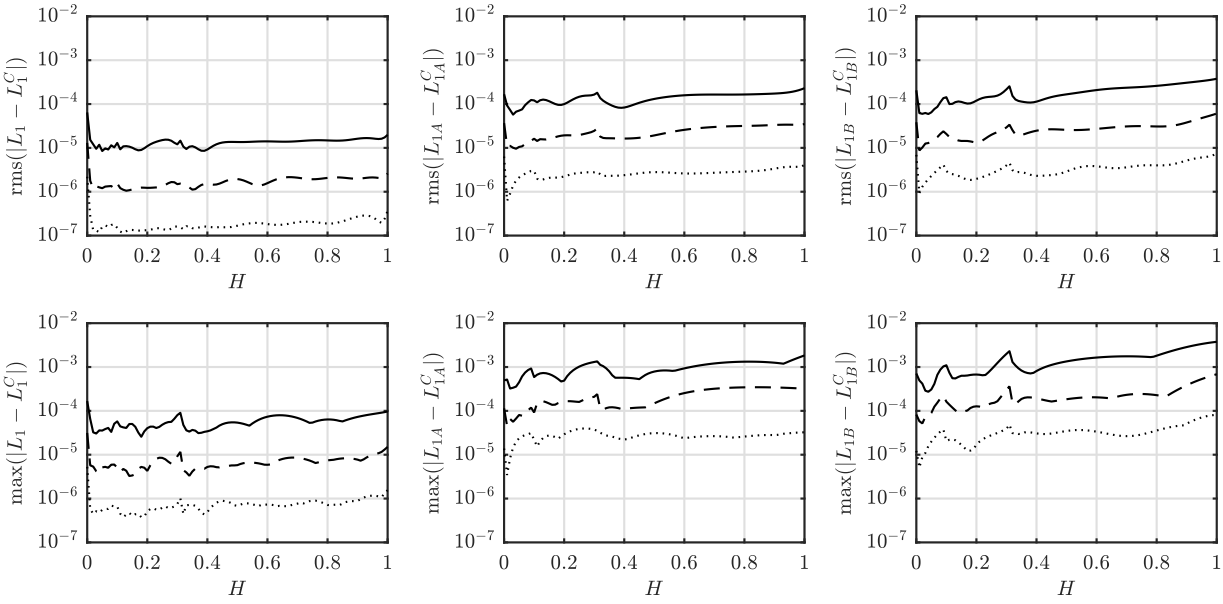

Fig. 10. RMS and maximum errors in Chebyshev approximation of L_1 and partial derivatives. Results shown for Chebyshev series truncated at $\min(|a_{pqr}|) < 10^{-5}$ (solid line), $\min(|a_{pqr}|) < 10^{-6}$ (dashed line) and $\min(|a_{pqr}|) < 10^{-7}$ (dotted line).

The integrals L_3 and M_3 are approximated in a similar way. For $H \in [1, 10]$ we map $\log_{10}(H)$ linearly onto $[-1, 1]$ with the domain split at $\log_{10}(H) = 0.5$. For $H > 10$ we map $1/H$ linearly onto $[-1, 1]$ and define $z = 20/H - 1$. The upper limits of the summations in each domain are $(N_p, N_q, N_r) = (10, 10, 13)$, $(11, 10, 13)$ and $(11, 10, 13)$ for L_3 and $(N_p, N_q, N_r) = (8, 8, 14)$, $(9, 9, 13)$ and $(7, 8, 7)$ for M_3. After summation over r, the number of terms with $|b_{pq}| > 10^{-7}$ in each subdomain are 79, 90 and 86 for L_3 and 49, 56 and 42 for M_3.

The errors in the approximation after truncating the Chebyshev series at various minimum values of $|a_{pqr}|$ are shown in Figs. 10–13. The maximum and root-mean-square (RMS) error over the $A - B$ plane are shown as a function of H. The RMS error is typically of the same order of magnitude as the minimum value of $|a_{pqr}|$ used, but the maximum error in the approximation is typically one order of magnitude larger than the minimum value of $|a_{pqr}|$. For the partial derivatives, the maximum and RMS errors are approximately an order of magnitude larger, since one term is lost in the series of the variable that is differentiated. For calculations involving elements of zero-thickness, the second-derivative of the Green function is also required (see e.g. [49]), which results in a further reduction in the accuracy of the approximation.

Newman [17] reported the use of around 8000 coefficients to approximate the integrals used in his method to 6-decimal accuracy in the region $H \in (0, \infty)$. The details of Newman's algorithm were not published, but from Figs. 10–13 we can infer that the stated 6-decimal accuracy is likely to require the use of coefficients down to a minimum absolute value $O(10^{-7})$. Similarly, Chen [18] reported the use of around 4900 coefficients to approximate the integrals used in his method to 6-decimal accuracy. The total number of coefficients in the Chebyshev approximations of L_j and M_j ($j = 1, 2, 3$), over all domains, with absolute values exceeding a minimum value is shown in Fig. 14. It is evident that only around 2200 coefficient are needed to achieve a similar level of accuracy for the expressions proposed here. Moreover, the inclusion of points for $H = 0$ and $1/H = 0$ allows the limiting forms of the Green function at zero and infinite frequency to be calculated using the same

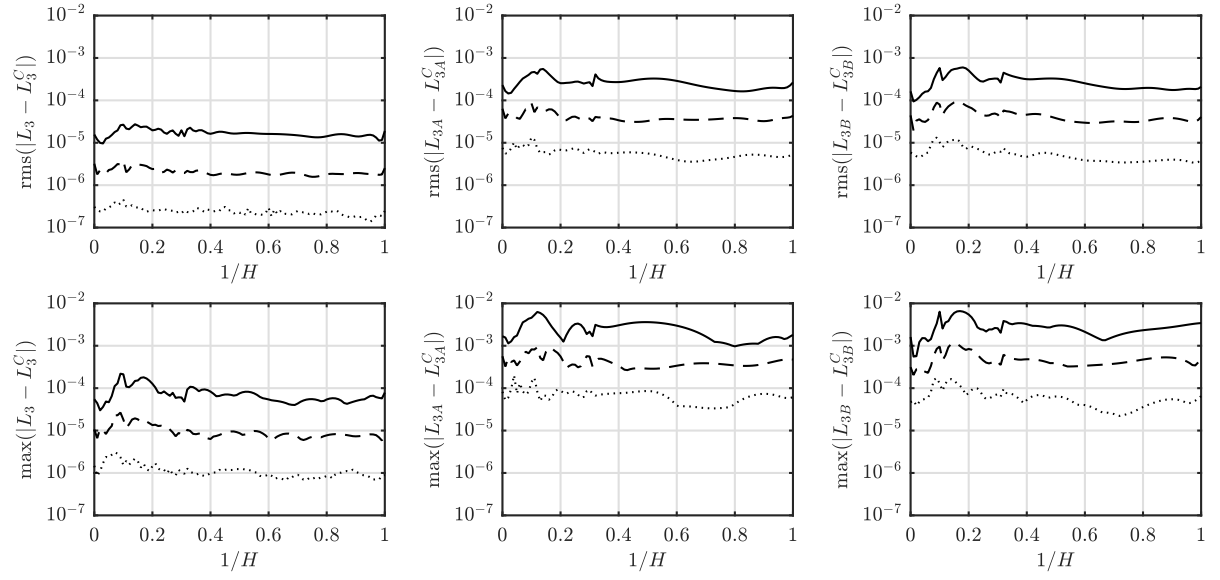

Fig. 11. As previous figure, but for L_3.

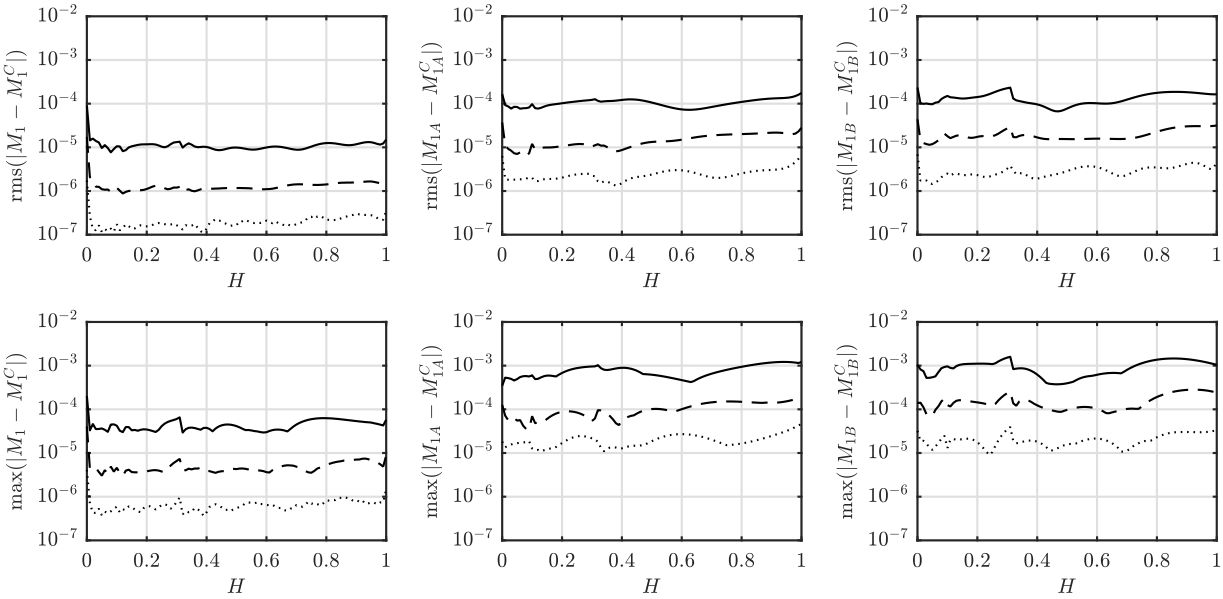

Fig. 12. As previous figure, but for M_1.

function used for positive finite frequencies.

MATLAB functions for calculating the Green function using the Chebyshev approximations described here are available at https://github.com/edmackay/GreenFunction. The Cheyshev coefficients a_{pqr} for each domain are stored up to a minimum absolute value of 10^{-7}, so that the user can select the level accuracy appropriate for their application.

7. Conclusions

New expressions for the free-surface Green function in finite water depth have been presented. In the near-field when $R/h \leq 1$ the Green function is expressed in terms of an integral, which is approximated using Chebyshev polynomials. In the mid- to far-field, when $R/h > 1$ the Green function is expressed using a modified form of the series defined by John [4]. The new expressions have the advantage that they are consistent with the limiting forms of the Green function for zero and infinite frequency. This removes the need to invoke a separate definition of the Green function at zero and infinite frequency, in terms of series of Rankine image sources, and enables a consistent definition to be used for the full range $K \in [0, \infty]$. It has also been demonstrated that the Fourier series representation of the zero and infinite frequency Green function derived by Newman [17] can be derived as the limiting forms of the series defined by John [4].

The new integral expressions have the further advantage that they are less variable with the non-dimensional frequency, Kh, than previous expressions proposed by Newman [14,17] and Chen [18]. To approximate the new expressions to an error of $O(10^{-6})$ using a truncated Chebyshev polynomial series, it was found that the number of terms required is reduced by factor of 4 compared to Newman's method and a factor of 2 compared to Chen's method.

Declaration of Competing Interest

The author confirm that there is no conflict of interest.

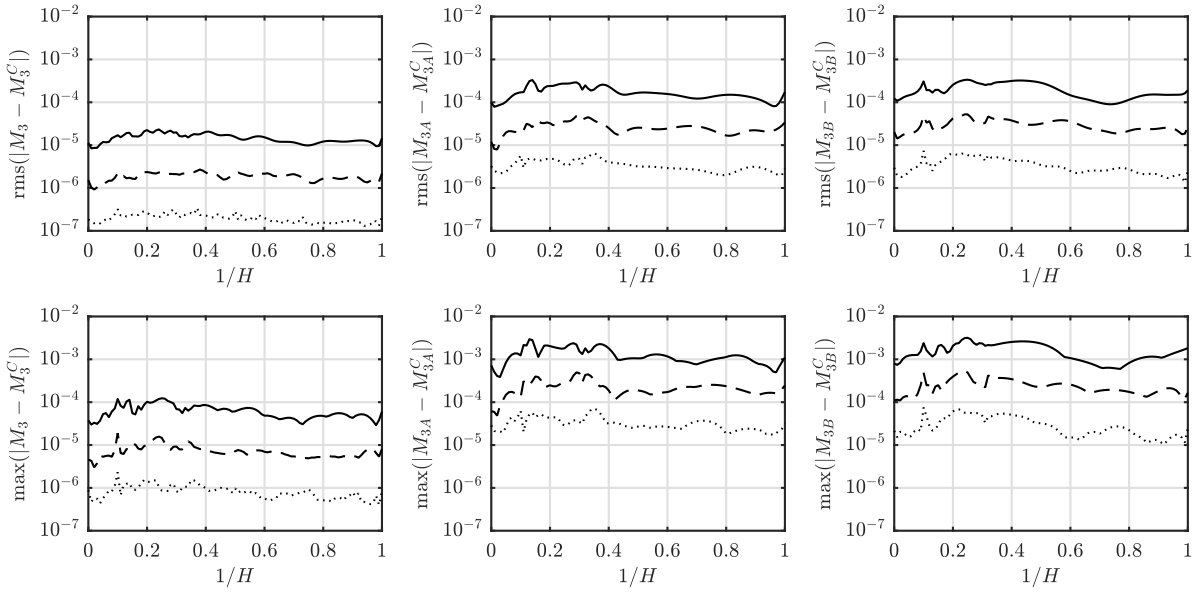

Fig. 13. As previous figure, but for M_3.

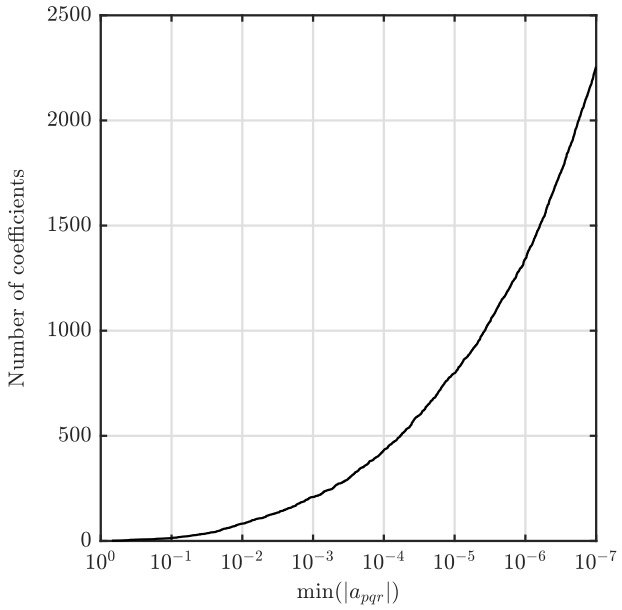

Fig. 14. Total number of Chebyshev coefficients over all domains against minimum value of $|a_{pqr}|$.

Acknowledgements

This work was funded under EPSRC grant EP/R007519/1.

Appendix A. Partial fraction expansion of $p(u, H)$

The function $p(u, H)$ defined in (71) is a meromorphic function of u with poles at the roots of $u\tanh(u) = H$, denoted $u = \pm u_n$, $n = 0, 1, 2, \cdots$, where u_0 is the positive real pole and u_n ($n \geq 1$) are the positive imaginary poles, ordered by increasing absolute value. The function is bounded for all complex u, excluding a small neighbourhood around the poles, and can therefore be represented by its partial fraction expansion (see e.g. [50]):

$$p(u, H) = \sum_{n=0}^{\infty} \frac{a_n}{u - u_n} + \frac{b_n}{u + u_n}, \tag{114}$$

where a_n and b_n are the coefficients corresponding to the poles at $u = \pm u_n$. As all the poles of $p(u, H)$ are simple poles, the coefficients a_n and b_n are the residues of $p(u, H)$ at $u = \pm u_n$, given by

$$a_n = \lim_{u \to u_n} (u - u_n)p(u, H) = \frac{u_n + H}{u_n \cosh(u_n) + (1 - H)\sinh(u_n)}, \tag{115}$$

$$b_n = \lim_{u \to -u_n} (u + u_n)p(u, H) = \frac{u_n - H}{u_n \cosh(u_n) + (1 - H)\sinh(u_n)}. \tag{116}$$

Gathering the terms in $\pm u_n$ we can write

$$p(u, H) = \sum_{n=0}^{\infty} c_n \frac{u + H}{u^2 - u_n^2}, \tag{117}$$

where

$$c_n = \frac{2u_n}{u_n \cosh(u_n) + (1 - H)\sinh(u_n)} = \frac{2u_n^2}{u_n^2 + (1 - H)H} \cdot \frac{1}{\cosh(u_n)}. \tag{118}$$

As $H \to 0$ we have $u_0 \to \sqrt{H}$ and $u_n \to in\pi$ ($n \geq 1$), so $c_0 \to 1$ and $c_n \to 2(-1)^n$, ($n \geq 1$). Therefore, as $H \to 0$ we have that

$$p(u, H) \to \frac{1}{2}\left(\frac{1 + \sqrt{H}}{u - \sqrt{H}} + \frac{1 - \sqrt{H}}{u + \sqrt{H}}\right) + 2\sum_{n=1}^{\infty} (-1)^n \frac{u + H}{u^2 + n^2\pi^2}. \tag{119}$$

Note that

$$2\sum_{n=1}^{\infty} \frac{(-1)^n}{u^2 + n^2\pi^2} = \frac{1}{u\sinh(u)} - \frac{1}{u^2}. \tag{120}$$

Therefore (119) can be rewritten as

$$p(u, H) \to \frac{1}{2}\left(\frac{1+\sqrt{H}}{u-\sqrt{H}} + \frac{1-\sqrt{H}}{u+\sqrt{H}}\right) + (u+H)\left(\frac{1}{u\sinh(u)} - \frac{1}{u^2}\right). \tag{121}$$

References

[1] C.-H. Lee, J. Newman, Computation of wave efects using the panel method, in: S. Chakrabarti (Ed.), Numerical Models in Fluid-Structure Interaction, 18 WIT Press, 2005, pp. 211–251, , https://doi.org/10.2495/978-1-85312-837-0/06.

[2] H. Maniar, A three dimensional higher-order panel method based on B-splines, MIT, Cambridge, Massachusetts, 1995 Ph.D. thesis.

[3] T. Havelock, The damping of the heaving and pitching motion of a ship, Lond. Edinb. Dublin Philos. Mag. J Sci. 33 (224) (1942) 666–673.

[4] F. John, On the motion of floating bodies II. Simple harmonic motion, Commun. Pure Appl. Math. 3 (1950) 45–101, https://doi.org/10.1002/cpa.3160030106.

[5] R. Thorne, Multipole expansions in the theory of surface waves, Math. Proc. Camb. Phil. Soc. 49 (4) (1953) 707–716.

[6] M. Haskind, On wave motion of a heavy fluid, Prikl. Mat. Mekh. 18 (1954) 15–26.

[7] T. Havelock, Waves due to a floating sphere making periodic heaving oscillations, Proc. Roy. Soc. A 231 (1955) 1–7.

[8] J.V. Wehausen, E. Laitone, Surface waves, Encycl. Phys. I (1960) 446–778, https://doi.org/10.5123/S1679-49742014000200017.

[9] W. Kim, On the harmonic oscillations of a rigid body on a free surface, J. Fluid Mech. 21 (1965) 427–451.

[10] G. Hearn, Alternative methods of evaluating Green's function in three-dimensional ship-wave problems, J. Ship Res. 21 (1977) 89–93.

[11] F. Noblesse, The Green function in the theory of radiation and diffraction of regular water waves by a body, J. Eng. Math. 16 (1982) 137–169.

[12] J.N. Newman, Double-precision evaluation of the oscillatory source potential, J. Ship Res. 28 (1984) 151–154.

[13] J.N. Newman, An expansion of the oscillatory source potential, Appl. Ocean Res. 6 (2) (1984) 116–117, https://doi.org/10.1016/0141-1187(84)90049-X.

[14] J.N. Newman, Algorithms for the free-surface Green function, J. Eng. Math. 19 (1) (1985) 57–67, https://doi.org/10.1007/BF00055041.

[15] J. Telste, F. Noblesse, Numerical evaluation of the Green function of water wave radiation and diffraction, J. Ship Res. 30 (2) (1986) 69–84.

[16] G. Delhommeau, Amélioration des performances des codes de calcul de diffraction-radiation au premier ordre, 2nd Journées de l'Hydrodynamique, Nantes, (1989), pp. 70–86.

[17] J.N. Newman, The approximation of free-surface Green functions, in: P.A. Martin, G.R. Wickham (Eds.), Wave Asymptotics, Cambridge University Press, 1992, pp. 107–135.

[18] X. Chen, Evaluation de la fonction de Green du probleme de diffraction/radiation en profondeur d'eau finie-une nouvelle methode rapide et precise, Actes des 4e Journees de l'Hydrodynamique, Nantes, France, (1993), pp. 371–384.

[19] B. Ponizy, F. Noblesse, M. Ba, M. Guilbaud, Numerical evaluation of free-surface Green functions, J. Ship Res. 38 (3) (1994) 193–202.

[20] M.A. Peter, M.H. Meylan, The eigenfunction expansion of the infinite depth free surface Green function in three dimensions, Wave Motion 40 (1) (2004) 1–11, https://doi.org/10.1016/j.wavemoti.2003.10.004.

[21] X. Yao, S. Sun, S. Wang, S. Yang, The research on the highly efficient calculation method of 3-D frequency-domain Green function, J. Marine Sci. Appl. 8 (3) (2009) 196–203, https://doi.org/10.1007/s11804-009-8035-y.

[22] J. D'elía, L. Battaglia, M. Storti, A semi-analytical computation of the Kelvin kernel for potential flows with a free surface, Comput. Appl. Math. 30 (2) (2011) 267–287, https://doi.org/10.1590/S1807-03022011000200002.

[23] A.H. Clément, A second order ordinary differential equation for the frequency domain Green function, Proceedings 28th International Workshop on Water Waves and Floating Bodies, Marseille, France, (2013).

[24] Y. Shen, D. Yu, W. Duan, H. Ling, Ordinary differential equation algorithms for a frequency-domain water wave Green's function, J. Eng. Math. 100 (1) (2016) 53–66, https://doi.org/10.1007/s10665-015-9833-7.

[25] H. Wu, C. Zhang, Y. Zhu, W. Li, D. Wan, F. Noblesse, A global approximation to the Green function for diffraction radiation of water waves, Eur. J. Mech. B/Fluids 65 (2017) 54–64, https://doi.org/10.1016/j.euromechflu.2017.02.008.

[26] H. Wu, H. Liang, F. Noblesse, Wave component in the Green function for diffraction radiation of regular water waves, Appl. Ocean Res. 81 (September) (2018) 72–75, https://doi.org/10.1016/j.apor.2018.10.006.

[27] H. Liang, H. Wu, F. Noblesse, Validation of a global approximation for wave diffraction-radiation in deep water, Appl. Ocean Res. 74 (2018) 80–86, https://doi.org/10.1016/j.apor.2018.02.025.

[28] C. Xie, Y. Choi, F. Rongère, A.H. Clément, G. Delhommeau, A. Babarit, Comparison of existing methods for the calculation of the infinite water depth free-surface Green function for the wave structure interaction problem, Appl. Ocean Res. 81 (September) (2018) 150–163.

[29] P. Shan, R. Zhu, F. Wang, J. Wu, Efficient approximation of free-surface Green function and OpenMP parallelization in frequency-domain wavebody interactions, J. Marine Sci. Technol. (Japan) 24 (2) (2018) 1–11, https://doi.org/10.1007/s00773-018-0568-9.

[30] C. Xie, X. Chen, A.H. Clément, A. Babarit, A new ordinary differential equation for the evaluation of the frequency- domain Green function, Appl. Ocean Res. 86 (February) (2019) 239–245, https://doi.org/10.1016/j.apor.2019.03.003.

[31] M.K. Pidcock, The calculation of Green's functions in three dimensional hydrodynamic gravity wave problems, Int. J. Numer. Methods Fluids 5 (10) (1985) 891–909, https://doi.org/10.1002/fld.1650051004.

[32] Y. Liu, H. Iwashita, C. Hu, A calculation method for finite depth free-surface Green function, Int. J. Naval Archit. Ocean Eng. 7 (2) (2015) 375–389, https://doi.org/10.1515/ijnaoe-2015-0026.

[33] M. Cuer, Computation of a Green's function for the three-dimensional linearized transient gravity waves problem, IMPACT Comput. Sci. Eng. 1 (3) (1989) 313–325, https://doi.org/10.1016/0899-8248(89)90015-3.

[34] C. Linton, Rapidly convergent representations for Green's functions for Laplace's equation, Proc. R. Soc. Lond. A 455 (1999) 1767–1797, https://doi.org/10.1098/rspa.1999.0379.

[35] H. LiuR.M., Ren, H.L., Li, An improved Gauss-Laguerre method for finite water depth Green function and its derivatives, J. Ship Res. 12 (2) (2008) 188–196.

[36] P. Yang, X. Gu, C. Tian, X. Cheng, J. Ding, Numerical study of 3D pulsating source Green function of finite water depth, International Conference on Offshore Mechanics and Arctic Engineering, (2014), https://doi.org/10.1115/OMAE2014-24703. V08BT06A061

[37] Z. Xie, Y. Liu, J. Falzarano, A more efficient numerical evaluation of the Green function in finite water depth, Ocean Syst. Eng. 7 (4) (2017) 399–412, https://doi.org/10.12989/ose.2017.7.4.399.

[38] Z. Chen, New formulation of the finite depth free surface Green functionarXiv:1808.07754v1(2018).

[39] W.E. Cummins, The impulse response function and ship motions, Schiffstechnik 9 (1962) 101–109.

[40] I.S. Gradshteyn, I.M. Ryzhik, Table of Integrals, Series, and Products, 7th edition, Academic Press, 2007.

[41] L.F. Shampine, Vectorized adaptive quadrature in MATLAB, J. Comput. Appl. Math. 211 (2) (2008) 131–140, https://doi.org/10.1016/j.cam.2006.11.021.

[42] C. Lee, J.N. Newman, X. Zhu, An extended boundary integral equation method for the removal of irregular frequency effects, Int. Jo. Numer. Methods Fluids 23 (January) (1996) 637–660.

[43] J.N. Newman, Distributions of sources and normal dipoles over a quadrilateral panel, J. Eng. Math. 20 (2) (1986) 113–126, https://doi.org/10.1007/BF00042771.

[44] J.N. Newman, P.D. Sclavounos, The computation of wave loads on large O shore structures, BOSS '88 Conference, Trondheim, Norway, (1988).

[45] Y. Liu, J.M. Falzarano, A method to remove irregular frequencies and log singularity evaluation in wave-body interaction problems, J. Ocean Eng. Mar. Energy 3 (2) (2017) 161–189, https://doi.org/10.1007/s40722-017-0080-z.

[46] M. Abramowitz, I. Stegun, Handbook of Mathematical Functions, United States Department of Commerce, National Bureau of Standards, 1964.

[47] C.C. Mei, M. Stiassnie, D.K.-P. Yue, Theory and Applications of Ocean Surface Waves, Advanced Series on Ocean Engineering 23 World Scientific, 2005, https://doi.org/10.1142/5566.

[48] J. Mason, D. Handscomb, Chevyshev Polynomials, Chapman & Hall/CRC, 2003.

[49] C.M. Linton, P. Mciver, Mathematical Techniques for Wave / Structure Interactions, Chapman & Hall/CRC, 2001.

[50] E. Freitag, R. Busam, Complex Analysis, Springer, 2005.